THERMAL FATIGUE FRACTURE CRITERIA
OF SINGLE CRYSTAL HEAT-RESISTANT ALLOYS
AND METHODS FOR IDENTIFICATION OF THEIR PARAMETERS

A. S. Semenov and L. B. Getsov   UDC 539.3

The deformation fracture criterion is introduced and its verification is performed on specimens from ZhS36 single crystal alloy with various crystallographic orientations under thermal fatigue testing with different temperatures and cycle durations.

Keywords: deformation criterion, thermal fatigue life, a single crystal material, crystallographic orientation.

Introduction. Due to wide application of single crystal materials in gas turbine industry for manufacturing of turbine blades, elaboration of adequate models of deformation and fracture criteria for static and especially thermocyclic loading is required. Multiple studies are dedicated to solving these problems [1–15]. Nevertheless, practical calculations are quite often based on deformation models of material, which are suitable only for polycrystalline blades, whereas thermal fatigue durability is estimated via the Manson formula for a universal inclination, which in many cases yields very big errors in the durability estimations.

The present work deals with the analysis of methods for assessing thermal fatigue durability of single crystal materials on the basis of application of deformation criteria with the account of crystallographic orientations (CGO), subdivision of contributions from cyclic and unilaterally accumulated (ratcheting) components of deformation, the separate account of influence of plastic deformations and creep deformations, which make it possible to adequately describe processes of thermal fatigue fracture of materials at complex variable disproportionate high-temperature loading taking into account presence of intermediate exposures. Verification of the developed methods is based on the results of thermal fatigue testing of specimens via the technique described in [8].

1. The Deformation Criterion Formulation. Process of damage accumulation in single crystal materials under thermocyclic loading includes parallelly developing stages: occurrence of slip bands; nucleation and development of microcracks; accumulation of irreversible deformations; formation and propagation of the main crack until fracture of the specimen (machine part). For forecasting the thermal fatigue failure of single crystal materials it is quite rational to use the modifications of the deformation criterion initially proposed in work [16]. As criterion of nucleation of macrocracks, the condition of achievement of the critical value by the total measure of damages is used, which is described by the following equation:

$$D = D_1 (\Delta\varepsilon_{eq}^p) + D_2 (\Delta\varepsilon_{eq}^c) + D_3 (\varepsilon_{eq}^p) + D_4 (\varepsilon_{eq}^c) = 1. \tag{1}$$

The proposed criterion (1) is based on linear summation of the damages caused by:
plastic deformation variations within a cycle

$$D_1 = \sum_{i=1}^{n} \frac{(\Delta\varepsilon_{eq_i}^p)^k}{C_1(T_i)}, \tag{2}$$

creep deformations within a cycle

$$D_2 = \sum_{i=1}^{n} \frac{(\Delta\varepsilon_{eq_i}^p)^m}{C_2(T_i)}, \tag{3}$$

unilaterally accumulated plastic deformation

$$D_3 = \max_{0 \leq t \leq t_{\max}} \frac{\varepsilon_{eq}^p}{\varepsilon_r^p(T)}, \tag{4}$$

and unilaterally accumulated creep deformation

$$D_4 = \max_{0 \leq t \leq t_{\max}} \frac{\varepsilon_{eq}^c}{\varepsilon_r^c(T)}, \tag{5}$$

where C_1, C_2, k, m, ε_r^p, and ε_r^c are the material parameters depending on temperature and CGO. Relations $k = 2$, $m = 5/4$, $C_1 = (\varepsilon_r^p)^k$, and $C_2 = [(3/4)\varepsilon_r^c]^m$ are frequently used, where ε_r^p and ε_r^c are limiting deformations of plasticity and creep under uniaxial tension.

As an equivalent measure of deformations ε_{eq}, various norms of deformation tensor can be considered in Eqs. (1)–(5):

the maximal shear deformation in the slip system with a normal to the slip plane $\mathbf{n}_{\{111\}}$ and slip direction $\mathbf{l}_{\langle 011 \rangle}$:

$$\varepsilon_{eq} = \mathbf{n}_{\{111\}} \varepsilon \mathbf{l}_{\langle 011 \rangle}, \tag{6}$$

the maximal principal strain (the maximum eigenvalue of deformation tensor):

$$\varepsilon_{eq} = \varepsilon_1, \tag{7}$$

strain intensity by Mises:

$$\varepsilon_{eq} = \sqrt{\frac{2}{9}\left[(\varepsilon_x - \varepsilon_y)^2 + (\varepsilon_y - \varepsilon_z)^2 + (\varepsilon_z - \varepsilon_x)^2 + \frac{3}{2}(\gamma_{xy}^2 + \gamma_{yz}^2 + \gamma_{zx}^2)\right]}, \tag{8}$$

and the maximal shear deformation:

$$\varepsilon_{eq} = \frac{1}{2}(\varepsilon_1 - \varepsilon_3). \tag{9}$$

The equivalent deformation (6) corresponds to crystallographic fracture mode, while the equivalent deformations (7)–(9) correspond to non-crystallographic fracture mode. The choice of the most suitable variant of the equivalent deformation on the basis of comparison of predicted life values with the experimental results was one of the conducted research tasks.

2. Experimental Results. Verification of the proposed deformation criterion (1) was performed on flat hour-glass type specimens from ZhS36 alloy with $\langle 001 \rangle$, $\langle 011 \rangle$, and $\langle 111 \rangle$ CGOs. Specimens with and without a central circular hole, which were loaded up to various levels of temperature with various cycle durations, were analyzed. Specimens were cut out from plates (Fig. 1) with various CGOs (Table 1).

It is noteworthy that usage of plates for manufacturing of specimens guarantees that these specimens have identical axial and azimuthal orientations, which is advantageous to the specimens made from circular bars, where coincidence of only axial orientations is provided, while inevitable variations in azimuthal orientation reduce accuracy of results obtained. Moreover, it is rather problematic to to produce specimens with fully conciding axial orientations.

TABLE 1. Crystallographic Orientations of Plates Used for Production of Specimens

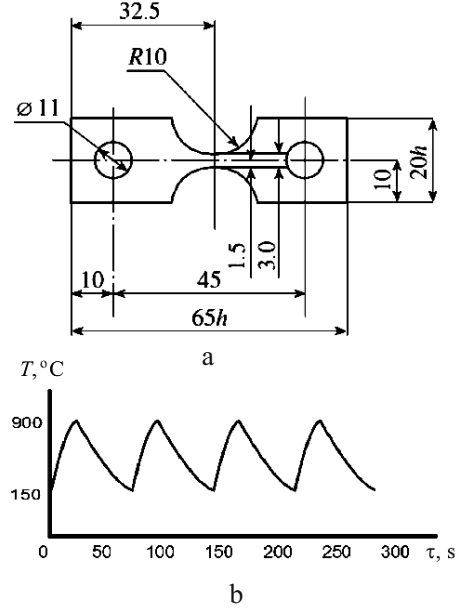| No. of plate	Orientation	Inclination from axial orientation, deg	Azymuthal orientation of micrographic plane, deg
1	$\langle 111 \rangle$	5.64	8.26
2	$\langle 011 \rangle$	4.51	11.27
3	$\langle 011 \rangle$	8.33	14.43
4	$\langle 011 \rangle$	9.67	7.86
5	$\langle 001 \rangle$	5.47	41.97

Fig. 1

Fig. 2

Fig. 1. Plates from which specimens are cut out.
Fig. 2. Test specimen (a) and temperature variation in its central part (b).

In tests, rigidly fixed specimens with a single polished surface are used. Specimen dimensions and characteristic variation of temperature in its central part are shown in Fig. 2. Tests were conducted in vacuum using loading modes with different maximum ($T_{max} = 900–1100°C$) and minimum ($T_{min} = 200–700°C$) temperatures in each cycle, which has made it possible to observe formation of slip bands, nucleation and propagation of cracks, as well as to measure their propagation rate on the specimen polished surface with optical magnification of ×250. Some specimens were subjected to exposure T_{max} with hold times of 2 and 5 minutes. Some specimens had stress concentrators in the form of central circular holes 0.5 mm in diameter. In order to define the CGO, a lowergramme was measured for each specimen, and calculations of Euler's angles φ, θ, and ψ, axial and azimuthal deviations, as well as the Schmid factor, were perfomed.

In the course of tests, relative axial displacements ΔK of two microhardness indentations, which have been made on the border of a working part of specimens with the distance of 4 mm from each other (Table 2), were measured per cycle. On the basis of the data obtained, the estimation of the range of axial mechanical deformations averaged within the specimen working part was conducted

Depending on the loading mode (the maximum temperature of a cycle and temperature range within a cycle), various fracture modes (crystallographic or non-crystallographic) were observed, which differed by orientation of fracture surfaces. An example of a map of fracture mechanisms for specimens of the third set is presented in Fig. 3.

Table 2 contains the experimental data on thermal fatigue life of single crystal specimens for various CGOs and loading modes, which are used for verification of the proposed deformation criterion (1).

TABLE 2. Thermal Fatigue Test Results for ZhS36 Alloy Specimens

Specimen set	CGO	$T_{\max}$, °C	$T_{\min}$, °C	Hold time, s	ΔK, μm	N_{in}, cycles	N_f, cycles
1-1c	⟨111⟩	900	150	–	12	10	50
1-2	⟨111⟩	900	150	–	15–18	190	823
1-5d	⟨111⟩	900	150	120	19–16	50	140
1-7d	⟨111⟩	900	150	300	16	10	16
1-6c	⟨111⟩	850	350	–	9	150	320
1-4cd	⟨111⟩	850	350	300	11	51–102	118
1-3d	⟨111⟩	1000	500	120	10	50–80	194
2-2	⟨011⟩	1000	500	–	14–12	300	472
2-5d	⟨011⟩	1000	500	300	10	200	317
2-1	⟨011⟩	900	150	–	18	17	100
2-4c	⟨011⟩	850	350	–	12–8	270	2952
2-6c	⟨011⟩	1000	500	–	10	10–130	187
2-3cd	⟨011⟩	1000	500	120	13, 11	1–2	62
3-0	⟨011⟩	900	150	–	22–14	730	951
3-1	⟨011⟩	950	200	–	18–12	52	450
3-2	⟨011⟩	1000	250	–	18	20	63
3-3	⟨011⟩	1000	500	–	11–8	455	1220
3-4	⟨011⟩	1050	550	–	20–17	160	356
3-5	⟨011⟩	950	450	–	14–11	1500	2535
4-1c	⟨011⟩	900	150	–	12	10	25
4-2	⟨011⟩	900	150	–	13	160	308
4-6d	⟨011⟩	900	150	120	13	6	17
4-4d	⟨011⟩	900	150	300	12	3	26
4-5	⟨011⟩	900	450	–	12–10	407	626
4-3d	⟨011⟩	900	450	120	13	90	128
5-1	⟨001⟩	900	150	–	13–10	435	560
5-2	⟨001⟩	1000	250	–	15	40–50	95
5-3	⟨001⟩	1000	500	–	13–7	305	1460
5-7cd	⟨001⟩	1000	500	–	9.5	8	344

Note. Set of specimens with stress concentrator is indicated by letter "c," set of specimens with hold time loading modes – by letter "d," N_{in} is number of cycles before main crack appearance, and N_f is number of cycles to final fracture of specimens.
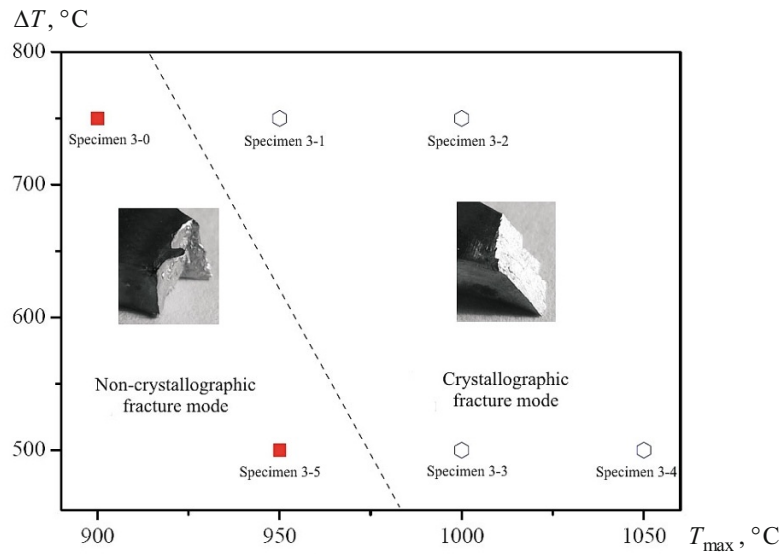

Fig. 3. Map of fracture mechanisms for specimens of the third set.

3. Governing Equations. In order to estimate the stress-strain state (SSS) of single crystal specimens sublected to complex programs of thermo-mechanical loading, it is expedient to apply physical models of inelastic deformation of the material, which take into account the fact that inelastic deformations occur according to the slip mechanism along the active slip systems and strongly depend on the chrystallographic orientation of a single crystal in relation to the direction of the external factor action. One should be very careful with application of plasticity and creep phenomenological models, which provide the account for anisotropy only for the criterion of plasticity and elastic properties.

It is assumed that plastic flow occurs as the result of possible slip along the octahedric slip systems N, which a characterized by a normal to αth slip plane $\mathbf{n}^\alpha$ and slip direction $\mathbf{l}^\alpha$ ($\alpha = 1, ..., N$). For the considered case of single crystals with face-centered cubic (fcc) lattice we have $N = 12$. The description of processes of inelastic deformation for finite deformations is based on application of the concept of multiplicate decomposition of the strain gradient $\mathbf{F}$ [2–7]:

$$\mathbf{F} = \mathbf{F}^* \mathbf{F}^p, \tag{10}$$

where the plastic component is controlled by the following equations:

$$\mathbf{L}^p = \dot{\mathbf{F}}^p \mathbf{F}^{p^{-1}} = \sum_{\alpha=1}^{N} \dot{\gamma}^\alpha \mathbf{l}^\alpha \mathbf{n}^\alpha, \tag{11}$$

$$\dot{\gamma}^\alpha = f(\tau^\alpha, ...), \tag{12}$$

$$\tau^\alpha = \sigma \cdot \mathbf{l}^\alpha \mathbf{n}^\alpha, \tag{13}$$

and the elastic one – by

$$\mathbf{E}^* = \frac{1}{2}(\mathbf{C} - \mathbf{1}) = \frac{1}{2}(\mathbf{F}^* \mathbf{F}^{*T} - \mathbf{1}), \tag{14}$$

$$S^* = {}^4\mathbf{D} \cdot \cdot \mathbf{E}^*. \tag{15}$$

Here $\dot{\gamma}^\alpha$ is speed/rate of slip in the α-slip system, which depends on the stressed state (shear stresses τ^α reduced to the given slip system), and can also depend on a number of internal variables, S^* is the Piola–Kirchhoff stress tensor of the 2nd type, which is related the Cauchi stress tensor σ via equality $S^* = J\mathbf{F}^{*-1} \sigma \mathbf{F}^{*-T}$, and $\mathbf{1}$ is a unit tensor. The choice of the particular form of expression (12) depends on the investigated phenomena (elastoplastic, viscoplastic, and viscoelastic behaviors), as well as on peculiarities of inelastic deformation of the considered single crystal.

For the viscous-elastic model used for the description of viscous effects in a single crystal below the yield stress level, calculation of multipliers $\dot{\gamma}^\alpha$, which characterize the intensity of inelastic deformation in the α-slip system, was made via the following equations:

$$\dot{\gamma}^\alpha = A|\tau^\alpha|^n (\gamma^\alpha)^m \operatorname{sign}(\tau^\alpha). \tag{16}$$

For the viscous-plastic model used for the description of viscous effects in a single crystal above the yield stress level, calculation of multipliers $\dot{\gamma}^\alpha$ was made as follows:

$$\dot{\gamma}^\alpha = \operatorname{sign}(\tau^\alpha - X^\alpha) \left\langle \frac{|\tau^\alpha - X^\alpha| - R^\alpha - \tau_0}{K} \right\rangle^n, \tag{17}$$

TABLE 3. Comparison of Experimental Data on Displacement of Base Points with the Calculated Results

Specimen set	CGO	T_{max}, °C	T_{min}, °C	Displacement of base points ΔK, μm		
				Calculation	Experiment	δ, %
1-2	$\langle 111 \rangle$	900	150	15.1	15–18	8
2-1	$\langle 011 \rangle$	900	150	18.3	18	2
2-2	$\langle 011 \rangle$	1000	500	17.4	12–14	34
2-4c	$\langle 011 \rangle$	850	350	5.6	8	30
2-6c	$\langle 011 \rangle$	1000	500	11.0	10	10
3-0	$\langle 011 \rangle$	900	150	19.3	14–22	7
3-2	$\langle 011 \rangle$	1000	250	17.1	18	5
3-4	$\langle 011 \rangle$	1050	550	19.5	17–20	5
3-5	$\langle 011 \rangle$	950	450	14.6	11–14	17
4-2	$\langle 011 \rangle$	950	450	14.1	13	7
4-5	$\langle 011 \rangle$	950	450	10.2	10–12	7
5-1	$\langle 001 \rangle$	900	150	10.2	10–13	11
5-2	$\langle 001 \rangle$	1000	250	13.9	15	13
5-3	$\langle 001 \rangle$	1000	500	10.2	7–13	2

where the variables characterizing isotropic and kinematic hardening are controlled by the following equalities:

$$R^\alpha = bQ\Sigma_\beta h^{\alpha\beta} r^\beta, \qquad \dot{r}^\alpha = (1 - br^\alpha)\dot{\gamma}^\alpha, \qquad h^{\alpha\beta} = H[q + (1 - q)\delta_{ab}], \qquad (18)$$

$$X^\alpha = Cx^\alpha, \qquad \dot{x}^\alpha = [\text{sign}\,(\tau^\alpha - X^\alpha) - Dx^\alpha]\dot{\gamma}^\alpha. \qquad (19)$$

In expression (17), the McOili brackets $\langle x \rangle = \begin{cases} x, & x \geq 0, \\ 0, & x < 0, \end{cases}$ are used. In Eqs. (16)–(19), A, n, m, τ_0, K, b, Q, H, q, C, and D are the material constants. Non-diagonal structure of a matrix $h^{\alpha\beta}$ makes it possible to consider two-way (latent) hardening of various slip systems.

For the elastoplastic model used for description of irreversible deformation effects under conditions of short-term loading of a single crystal above the yield stress level, calculation of multipliers $\dot{\gamma}^\alpha$ was based on the following equations:

$$f^\alpha = |\tau^\alpha - X^\alpha| - R^\alpha - \tau_0 = 0, \qquad (20)$$

where the variables characterizing isotropic and kinematic hardening are controlled by Eqs. (18) and (19). Multipliers $\dot{\gamma}^\alpha$ are determined as solutions of a system of nonlinear algebraic equations, which are derived from (20), (13), (18), and (19).

The further refinement of models can be achieved by incorporation of densities of mobile dislocations and the equations of their evolution [17] into the hardening laws.

For verification of accuracy of solutions using physical models we compared the experimental data on relative displacement within a cycle of specimen basic points (two microhardness indenations) with the calculated ones. Comparison of the experimental data for specimens with no hold time with calculations via the elastoplastic model has shown their good fit (Table 3), while the accuracy of calculations made via viscous-plastic models with account of hold time is somewhat lower, which is attributed to insufficient volume of the input data on creep in the total temperature range.

4. Deformation Criterion Verification. Thermocyclic loading, which provides spatially nonuniform and nonstationary temperature field, generates non-uniform stress and strain fields in flat hour-glass type specimens from single crystal alloy, both with and without central hole. A possibility of arbitrary orientation of anisotropic material (for the cubic symmetry group) in relation to geometrical axes of the specimen and strongly pronounced
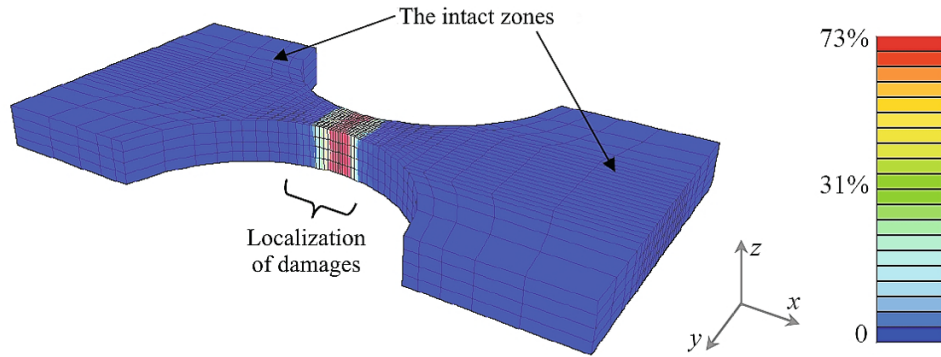
Fig. 4. Distribution of the damage field after the tenth thermal cycle for specimen 5-1 with $\langle 001 \rangle$ orientation.
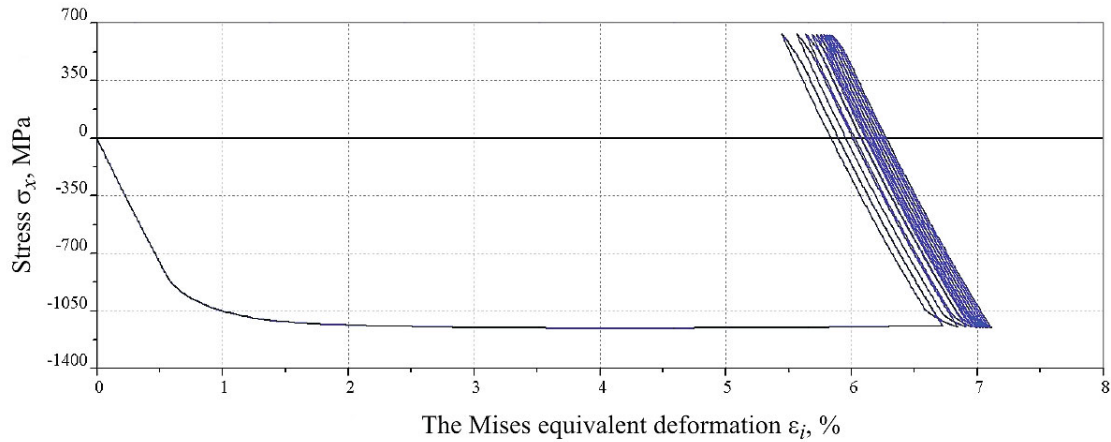

Fig. 5. Cyclic deformation curve for the central point of specimen 5-1.

physically nonlinear behavior also complicates the problem of deriving simple analytical estimations of the SSS. Therefore for definition of the SSS of specimens we used finite element (FE) solutions in three-dimensional statement with application of inelastic models of the material described in Section 3.

Analysis of the SSS and processes of damage accumulation in hour-glass type specimens was performed using the FE software program complex PANTOCRATOR [18]. Application in calculations of physical models of a material allows one to take into account that inelastic deformations occur according to the slip mechanism along active slip systems and strongly depend on the single crystal crystallographic orientation in relation to the direction of external factor action. In the numerical experiments we used the elastoplastic and viscoelastoplastic material models [6, 7] with nonlinear kinematic and isotropic hardening, as well as those with auto-hardening and wo-way (latent) hardening of various slip systems. It has been established that application of viscoelastic models provides unrealistically overestimated stress levels.

The FE calculation results obtained as solutions of three-dimensional nonlinear boundary problems with characteristic non-uniform fields of stresses, strains and damages allow one to determine sites of the most loaded points of the specimen, which are the most probable origins of nucleation of cracks. A typical distribution of the field of damages with use of criterion (1) after the tenth thermal cycle $(20 \rightarrow T_{\max} = 900 \leftrightarrow T_{\min} = 150°C)$ for specimen 5-1 from ZhS36 alloy with the orientation close to $\langle 001 \rangle$ is presented in Fig. 4. The corresponding curve of cyclic deformation for the central point of specimen 5-1 is shown in Fig. 5.

Verification of deformation criterion (1) was conducted with use of the experimental data on creep and curves of elastoplastic deformation of ZhS36 alloy [11] on the basis of the FE calculations executed for each specimen taking into account its CGO and the loading mode. Calculations were carried out by the direct step-by-step modeling of cycle-by-cycle kinetics of deformations with automatic determination of damage field variation in the process of problem solving. The number of cycles to formation of the main crack, calculated on the basis of criterion (1) with

TABLE 4. Comparison of Experimental Data on Life with the Experimental Results

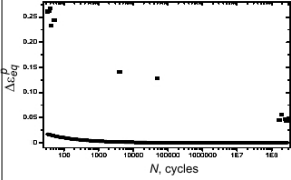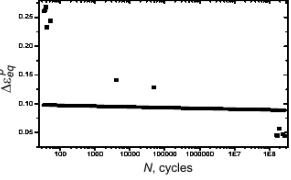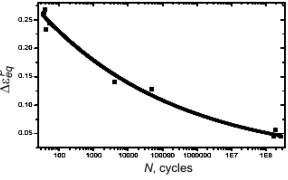| Specimen set	CGO	T_{max}, °C	T_{min}, °C	ΔT, °C	N_{in}, cycles					
					$\varepsilon_{eq} = \varepsilon_{n1}$ (6)	$\varepsilon_{eq} = \varepsilon_1$ (7)	$\varepsilon_{eq} = \varepsilon_i$ (8)	$\varepsilon_{eq} = \gamma_{max}$ (9)	Experiment	δ, %
1-1c	$\langle 111 \rangle$	900	150	750	5	4	3	4	10	50
1-2	$\langle 111 \rangle$	900	150	750	28	19	21	25	190	85
1-5d	$\langle 111 \rangle$	900	150	750	36	13	20	24	50	28
1-6c	$\langle 111 \rangle$	850	350	500	11	8	7	8	45	93
2-1	$\langle 011 \rangle$	900	150	750	15	9	10	15	17	12
2-2	$\langle 011 \rangle$	1000	500	500	444	340	248	431	300	15
2-4c	$\langle 011 \rangle$	850	350	500	34	28	28	29	210	84
2-6c	$\langle 011 \rangle$	1000	500	500	61	44	56	57	10–130	13
3-0	$\langle 011 \rangle$	900	150	750	17	2	11	17	100	83
3-1	$\langle 011 \rangle$	950	200	750	12	3	7	12	52	77
3-2	$\langle 011 \rangle$	1000	250	750	9	2	5	9	35	74
3-3	$\langle 011 \rangle$	1000	500	500	550	494	328	540	250	120
3-4	$\langle 011 \rangle$	1050	550	500	365	293	172	358	160	128
3-5	$\langle 011 \rangle$	950	450	500	866	538	580	866	1500	42
4-1c	$\langle 011 \rangle$	900	150	750	6	4	4	5	10	40
4-2	$\langle 011 \rangle$	950	450	500	24	15	17	21	160	85
4-5	$\langle 011 \rangle$	950	450	500	86	25	8	85	360	76
4-6d	$\langle 011 \rangle$	900	150	750	8	6	5	7	6	33
5-1	$\langle 001 \rangle$	900	150	750	338	275	195	280	435	22
5-2	$\langle 001 \rangle$	1000	250	750	94	473	28	68	55	71
5-3	$\langle 001 \rangle$	1000	500	500	218	196	150	172	305	29
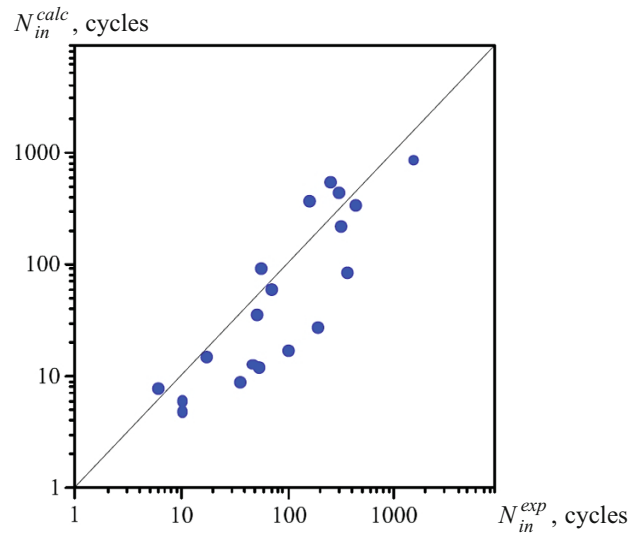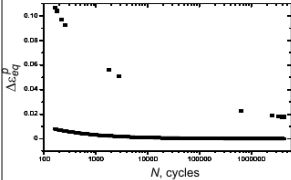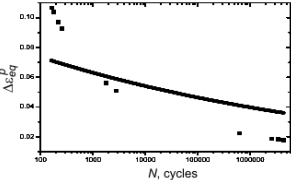
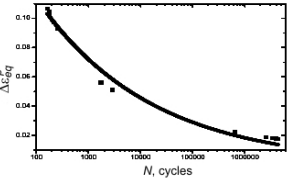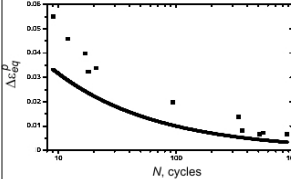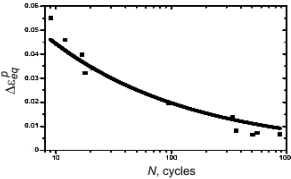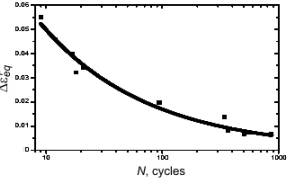Fig. 6. Comparison of the calculated number of cycles N_{in}^{calc} to formation of the main crack with use of criterion (1)–(6) with the experimental results N_{in}^{exp}.

use of the equivalent deformations (6)–(9), are presented in Table 4. The best accuracy, in comparison with the experimental results, is provided by the criterion with use of the equivalent deformation, which accounts for crystallographic orientation (6), as is shown in Table 4. For criterion (1), the maximum relative error δ in the life predictions does not exceed 130%, an average error being 60%. In case where the fracture criterion is based on the Mises deformation intensities (8), the most conservative estimation is obtained. A close correlation between the results of calculations via (1)–(6) and the experimental values is observed, as is shown in Fig. 6.

TABLE 5. Comparison of Criteria for Various Ways of Determination of Parameters k and ε_r

Criterion	$\varepsilon_r = \varepsilon_r^{p*}$, $k = 2$	$\varepsilon_r = \varepsilon_r^{p*}$, $k = \text{var}$	$\varepsilon_r = \text{var}$, $k = \text{var}$
By Coffin (22)	$\chi_{red}^2 = 9 \cdot 10^{-1}$	$\chi_{red}^2 = 1.2 \cdot 10^{-2}$	$\chi_{red}^2 = 9.8 \cdot 10^{-5}$
By Manson (23)	$\chi_{red}^2 = 1 \cdot 10^{-1}$	$\chi_{red}^2 = 6 \cdot 10^{-4}$	$\chi_{red}^2 = 2.2 \cdot 10^{-5}$
(21)	$\chi_{red}^2 = 6.4 \cdot 10^{-4}$	$\chi_{red}^2 = 1.8 \cdot 10^{-5}$	$\chi_{red}^2 = 6.8 \cdot 10^{-6}$

Note. Lines depict results of approximation of the experimental data (given as points).

5. Comparison of the Results Obtained via Criteria (1)–(6) with Predictions by Other Criteria. Let us compare the results obtained using the proposed criterion (1)–(6) with forecasts made via the Coffin and the Manson criteria. We will limit our consideration to the case of short-term loading with on account of contributions from creep deformations. In this case, the deformation criterion (1)–(6) can be reduced to its simplified representation:

$$\sum_{j=1}^{N}\left(\frac{\Delta\varepsilon_{eq}^p}{\varepsilon_r}\right)^k + \frac{\max\varepsilon_{eq}^p}{\varepsilon_r} = 1. \tag{21}$$

The Coffin criterion is described by the following equality:

$$\sum_{j=1}^{N}\left(\frac{\Delta\varepsilon_{eq}^p}{\varepsilon_r}\right)^k = 1. \tag{22}$$

The Manson criterion of universal inclinations is given as follows:

$$\Delta\varepsilon_{eq}^p = 1.75\frac{\sigma_u}{E}N^{-0.12} + \varepsilon_r N^{-0.6}, \tag{23}$$

where σ_u is the tensile ultimate strength and E is the elastic module.

Comparison of criteria was performed on the basis of the analysis of the root-mean-square deviation values χ_{red}^2 of the approximating dependences (21)–(23) derived during determination of constants k and ε_r by the least squares technique (minimization of χ_{red}^2). Results of comparison are presented in Table 5 for three ways of

identification of constants: with the fixed values $k = 2$ and $\varepsilon_r = \varepsilon_r^{p^*}$ ($\varepsilon_r^{p^*}$ is the limiting plastic deformation under tensile loading), with the fixed value $\varepsilon_r = \varepsilon_r^{p^*}$ and variable value k, and with two variable parameters k and ε_r.

The results of comparing the criteria of macrocracks' initiation under thermal fatigue conditions for the considered class of problems using various ways of determination of constants show that the most exact solution is provided by the combined criterion (21). However, this conclusion requires further experimental verification for various loading conditions and other single crystal alloys.

Conclusions. Various modifications of deformation-based fracture criterion for single crystal alloys under thermocyclic loading conditions are proposed. Verification of the criterion for single crystal ZhS36 alloy is presented on the basis of comparison with the experimental data obtained on hour-glass type specimens with various orientation of crystallographic axes ($\langle 001 \rangle$, $\langle 011 \rangle$, and $\langle 111 \rangle$) at different temperatures (150–1050°C) and cycle durations (20–385 s). A high accuracy of thermal fatigue life prediction by means of the proposed criterion is established.

The importance of taking into account the unilaterally accumulated inelastic deformation along with its range within a cycle is demonstrated in calculations of the number of cycles to macrocrack initiation. It is established that usage in the fracture criterion of the equivalent deformations related to the maximum shear in the slip planes, yields more exact life forecast, than usage of the equivalent deformations which prproved no explicit account of the crystallographic orientations. Application of the Mises deformation intensities results in the most conservative estimation.

For determination of the stress-strain state of single crystal specimens we have executed FE calculations by means of physical models of plasticity and creep by postulating that inelastic deformation of a single crystal occurs according to the available active slip systems and is controlled by the crystallographic orientation. Distribution of damage fields in the specimen and history of their variation are analyzed, which allows one to directly identify the potential initiation sites of thermal fatigue macrocracks, as well as to estimate the respective number of cycles to initiation. As a result of combined experimental and calculation studies, a strongly pronounced sensitivity of thermal fatigue life of single crystals to crystallographic orientation of specimens is proved.

The results obtained are recommended to be used in calculations of thermal fatigue life of gas turbine blades produced from single crystal alloys.

REFERENCES

1. L. B. Getsov and V. E. Mikhailov, A. S. Semenov, et al., "Residual life calculation of operating and guiding gas turbine blades. Pt. 2. Single crystal materials," *Gazoturb. Tekhnol.*, No. 8, 18–25 (2011).
2. R. Hill, "Generalized constitutive relations for incremental deformation of metal crystals by multislip," *J. Mech. Phys. Solids*, **14**, 95–102 (1966).
3. R. Hill and J. R. Rice, "Constitutive analysis of elastic-plastic crystals at arbitrary strains," *J. Mech. Phys. Solids*, **20**, 401–413 (1972).
4. R. J. Asaro and J. R. Rice, "Strain localisation in ductile single crystals," *J. Mech. Phys. Solids*, **25**, 309–338 (1977).
5. R. J. Asaro, "Crystal plasticity," *J. Appl. Mech.*, **50**, 921–934 (1983).
6. G. A. Cailletaud, "Micromechanical approach to inelastic behaviour of metals," *Int. J. Plast.*, **8**, 55–73 (1991).
7. J. Besson, G. Cailletaud, J.-L. Chaboche, and S. Forest, *Non-Linear Mechanics of Materials*, Springer (2010).
8. L. B. Getsov, N. I. Dobina, A. I. Rybnikov, et al., "Thermal fatigue resistance of a monocrystalline alloy," *Strength Mater.*, **40**, No. 5, 538–551 (2008).

9. L. Getsov, A. Semenov, and A. Staroselsky, "A failure criterion for single-crystal superalloys during thermocyclic loading," *Mater. Technol*., **42**, No. 1, 3–12 (2008).

10. L. B. Getsov, A. I. Rybnikov, and A. S. Semenov, "Thermal fatigue resistance of heat-resistant alloys," *Teploénergetika*, No. 5, 51–58 (2009).

11. L. B. Getsov, A. I. Rybnikov, A. S. Semenov, et al., "Deformation resistance and fracture toughness of single-crystal alloys under static and termocyclic loading," *Nadezhn. Bezopasn. Énerg*., No. 18, 53–62 (2012).

12. E. N. Kablov and E. R. Golubovskii, *Thermal Stability of Nickel Alloys* [in Russian], Mashinostroenie, Moscow (1998).

13. R. E. Shalin, I. L. Svetlov, E. B. Kachanov, et al., *Single Crystals of Nickel Superalloys* [in Russian], Mashinostroenie, Moscow (1997).

14. N. K. Arakere and G. Swanson, "Effect of crystal orientation on fatigue failure of single crystal nickel base turbine blade superalloys," *Int. J. Eng. Gas Turbines Power*, **124**, 161–176 (2002).

15. A. Garcia de la Yedra, A. Martin-Meizoso, R. Rodriguez Martin, and J. L. Pedrejon, "Thermo-mechanical fatigue behaviour and life prediction of C-1023 nickel based superalloy," *Int. J. Eng. Sci. Technol.*, **3**, No. 6, 88–101 (2011).

16. L. B. Getsov, "On fracture criterion for complex program loading," in: Proc. All-Union Workshop on *Low-Cycle Fatigue Problems* [in Russian], Kaunas (1971).

17. R. M. Odobai-Fard, A. S. Semenov, and L. B. Getsov, "Modeling of processes of inelastic deformation of specimens from single-crystal materials with account of dislocations' dynamics," in: Proc. Int. Conf. *"XL Week of Science in St. Petersburg State Polytechnical University"* [in Russian], Part V, St. Petersburg (2011), pp. 72–73.

18. A. S. Semenov, "PANTOCRATOR – a finite-element program specialized on the solution of nonlinear problems of solid-mechanics," in: Proc. of the 5th Int. Conf. *"Scientific and Engineering Problems of Predicting the Reliability and Service Life of Structures and Methods of Their Solution"* [in Russian], SPbGPU, St. Petersburg (2003), pp. 466–480.